Adiabatic self-tuning in a silicon microdisk optical resonator

Q. Lin, T. J. Johnson, C. P. Michael, and O. Painter

Department of Applied Physics, California Institute of Technology, Pasadena, CA 91125

linq@caltech.edu

Abstract: We demonstrate a method for adiabatically self-tuning a silicon microdisk resonator. This mechanism is not only able to sensitively probe the fast nonlinear cavity dynamics, but also provides various optical functionalities like pulse compression, shaping, and tunable time delay.

OCIS codes: (190.4390) Nonlinear optics, integrated optics; (130.3990) Micro-optical devices; (230.5750) Resonators; (320.5550) Pulses.

References and links

1. E. J. Reed, M. Soljacic, and J. Joannopoulos, "Color of shock waves in photonic crystals," Phys. Rev. Lett. **90**, 203904 (2003).
2. M. F. Yanik and S. Fan, "Stopping light all optically," Phys. Rev. Lett. **92**, 083901 (2004).
3. M. Notomi and S. Mitsugi, "Wavelength conversion via dynamic refractive index tuning of a cavity," Phys. Rev. A **73**, 051803(R) (2006).
4. M. Notomi, H. Taniyama, S. Mitsugi, and E. Kuramochi, "Optomechanical wavelength and energy conversion in high-Q double-layer cavities of photonic crystal slabs," Phys. Rev. Lett. **97**, 023903 (2006).
5. Z. Gaburro, M. Ghulinyan, F. Riboli, L. Pavesi, A. Recati, and I. Carusotto, "Photon energy lifter," Opt. Express **14**, 7270–7278 (2006).
6. S. F. Preble, Q. Xu, and M. Lipson, "Changing the colour of light in a silicon resonator," Nature Photon. **1**, 293–296 (2007).
7. M. W. McCutcheon, A. G. Pattantyus-Abraham, G. W. Rieger, and J. F. Young, "Emission spectrum of electromagnetic energy stored in a dynamically perturbed optical microcavity," Opt. Express **15**, 11472–11480 (2007).
8. P. Dong, S. F. Preble, J. T. Robinson, S. Manipatruni, and M. Lipson. "Introducing photonic transitions between discrete modes in a silicon optical microcavity," Phys. Rev. Lett. **100**, 033904 (2008).
9. A. M.Yacomotti, F. Raineri, C. Cojocaru, P. Monnier, J. A. Levenson, and R. Raj, "Nonadiabatic dynamics of electromagnetic field and charge carriers in high-Q photonic crystal resonators," Phys. Rev. Lett. **96**, 093901 (2006).
10. T. Tanabe, M. Notomi, E. Kuramochi, A. Shinya, and H. Taniyama, "Trapping and delaying photons for one nanosecond in an ultrasmall high-Q photonic-crystal nanocavity," Nature Photon. **1**, 49–52 (2007).
11. Y. Tanaka, J. Upham, T. Nagashima, T. Sugiya, T. Asano, and S. Noda, "Dynamic control of the Q factor in a photonic crystal nanocavity," Nature Mater. **6**, 862–865 (2007).
12. Q. Lin, O. J. Painter, and G. P. Agrawal, "Nonlinear optical phenomena in silicon waveguides: Modeling and applications," Opt. Express **15**, 16604–16644 (2007).
13. M. Borselli, T. J. Johnson, C. P. Michael, M. D. Henry, and O. Painter, "Encapsulation layers for low-loss silicon photonics," Appl. Phys. Lett. **91**, 131117 (2007).
14. M. Borselli, T. J. Johnson, and O. Painter, "Beyond the Rayleigh scattering limit in high-Q silicon microdisks: theory and experiment," Opt. Express **13**, 1515–1530 (2005).
15. T. J. Johnson, M. Borselli, and O. J. Painter, "Self-induced optical modulation of the transmission through a high-Q silicon microdisk resonator," Opt. Express **14**, 817–831 (2006).
16. T. J. Kippenberg, S. M. Spillane, and K. J. Vahala, "Mode coupling in traveling-wave resonators," Opt. Lett. **27**, 1669–1671 (2002).
17. The intrnsic Q factor is referred to that originated from the intrnisic loss of the microdisk, while the loaded one is referred to that for the microdisk loaded with the coupling fiber taper. See Ref. [14].
18. P. E. Barclay, K. Srinivasan, and O. Painter, "Nonlinear response of silicon photonic crystal micresonators excited via an integrated waveguide and fiber taper," Opt. Express **13**, 801–820 (2005).

#98656 - $15.00 USD Received 11 Jul 2008; revised 1 Sep 2008; accepted 1 Sep 2008; published 4 Sep 2008

19. R. A. Soref and B. R. Bennett, "Electrooptical effects in silicon," IEEE J. Quantum Electron. **23**, 123–129 (1987).
20. R. W. Boyd and D. J. Gauthier, "Slow and fast light," in *Progress in Optics*, Vol. 43, E. Wolf, ed. (Elsevier, 2002).
21. J. B. Khurgin, "Optical buffers based on slow light in electromagnetically induced transparant media and coupled resonator structures: comparative analysis," J. Opt. Soc. Am. B **22**, 1062–1074 (2005).
22. E. Tien, N. S. Yuksek, F. Qian, and O. Boyraz, "Pulse compression and mode locking by using TPA in silicon waveguides," Opt. Express **15**, 6500–6506 (2007).
23. A. Liu, R. Jones, L. Liao, D. Samara-Rubio, D. Rubin, O. Cohen, R. Nicolaescu, M. Paniccia, "A high-speed silicon optical modulator based on a metaloxidesemiconductor capacitor," Nature **427**, 615–618 (2004).
24. Q. Xu, B. Schmidt, S. Pradhan, and M. Lipson, "Micrometre-scale silicon electro-optic modulator," Nature **435**, 325–327 (2005).

1. Introduction

Dynamic control of high-quality (high-Q) microcavities has attracted considerable interest in the past few years because of its remarkable capabilities for manipulating photon properties [1–5]. It has been used recently to demonstrated frequency conversion [6–8] and fast tuning of cavity Q [9–11] in semiconductor microcavities by externally tuning the cavity resonance with intense femtosecond pulses. Here we propose and demonstrate an approach for adiabatic tuning of high-Q microcavities that is realized in an intrinsic fashion by launching an optical pulse with only moderate peak power into a cavity resonance. Such self-tuning exhibits unique temporal and spectral characteristics which are able to sensitively probe the fast nonlinear cavity dynamics within the photon lifetime. It also provides novel optical functionalities like temporal compression, shaping, and tunable delay of optical pulses which may find applications in future high-speed optical signal processing on a chip scale.

When an optical pulse is launched into a resonance of a high-Q silicon microcavity, its leading edge fed into the cavity builds up constructively and leads to a dramatic increase of intracavity power to a level orders of magnitude higher than the input. For an optical wave in the telecom band that is above the half band gap of silicon, high intracavity powers introduce significant two-photon absorption (TPA) and generate a considerable number of free carriers. As the carrier generation rate is proportional to the square of the intracavity power [12], the carrier density increases rapidly on a time scale much shorter than the power buildup. The resulting plasma-dispersion effect then dynamically tunes the cavity resonance within the photon lifetime. On the one hand, such adiabatic tuning of the cavity resonance shifts the trapped photons towards higher frequencies. As the input wave continuously feeds the cavity, photons with different frequencies simultaneously circulate inside the cavity and beat with each other, leading to substantial temporal modulation in the total intracavity power. On the other hand, the dynamic tuning of the cavity resonance away from the input frequency also quenches further power feeding from the incident wave, effectively leaving only a short duration of the pulse circulating inside the cavity. As a result, a short pulse is generated at the drop port of the resonator, whose temporal shape is predefined by the cavity tuning dynamics and the peak power of the incident wave.

2. Experimental configuration

We employ a high-Q silicon microdisk to demonstrate such phenomena. It consists of a 202-nm thick silicon layer with a diameter of 20 μm sitting on a 2-μm-high partially undercut silica pedestal. Its surface is passivated with a 15-nm SiO_2 cap layer to reduce the absorption by surface states [13]. The microdisk is fabricated through a procedure optimized to realize a high Q factor up to the order of 10^6 [14, 15]. For such a high-Q mode, Rayleigh scattering (due to surface roughness of the disk) from the forward whispering gallery mode (WGM) couples a certain amount of optical power into the backward WGM inside the microdisk. Such mode coupling splits the resonant mode into a doublet [14, 16], and provides a unique probing tool for investi-

#98656 - $15.00 USD Received 11 Jul 2008; revised 1 Sep 2008; accepted 1 Sep 2008; published 4 Sep 2008

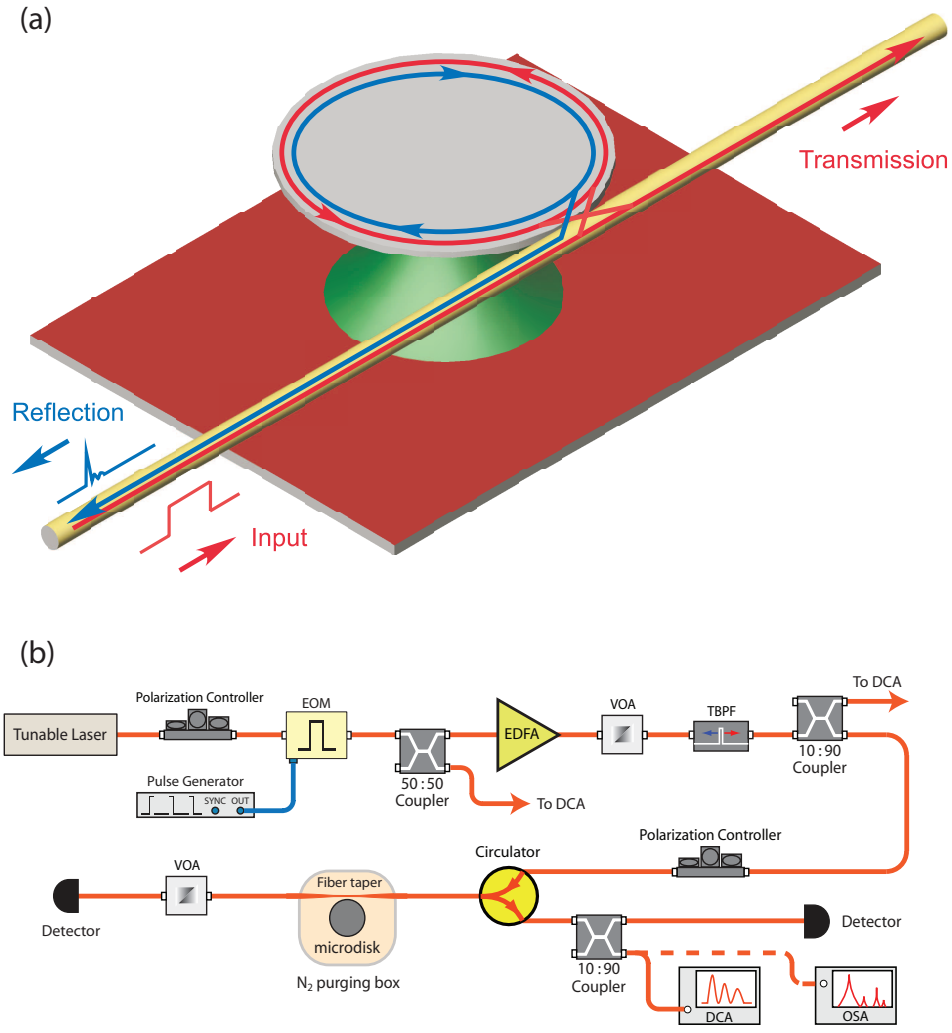

Fig. 1. (a) Schematic of the cavity self-tuning experiment. The input optical pulse is launched into the microdisk through a fiber taper, which excites adiabatic self-tuning of cavity resonance. The backward WGM couples back to the fiber taper as the reflection wave. (b) Experimental setup. EOM: electro-optic modulator. EDFA: erbium-doped fiber amplfier. VOA: variable optical attenuator. TBPF: tunable bandpass filter. DCA: digital communication analyzer. OSA: optical spectrum analyzer.

gating the cavity dynamics through the backward channel. The input optical pulses are launched into the microdisk through a single-mode fiber taper with a diameter of $\sim 1\ \mu$m, which simultaneously collects the reflected wave coupled from the backward WGM [see Fig. 1(a)]. The fiber taper functions simultaneously as the input, transmitted, and drop ports of the resonator. It is maintained in contact with the microdisk for stable coupling. We use TE-like resonances for observing the tuning phenomena because of their high mode confinement inside the thin silicon microdisk.

Figure 1(b) shows our experimental setup. the continuous-wave output of a tunable laser is modulated by a lithium niobate eletro-optic modulator to obtain square pulses with a rise and

#98656 - $15.00 USD Received 11 Jul 2008; revised 1 Sep 2008; accepted 1 Sep 2008; published 4 Sep 2008

fall time (10%-90%) of 123 and 200 ps, respectively. The pulses are amplified by an erbium-doped fiber amplifier (EDFA) to boost its peak power and are subsequently filtered by a tunable band-pass filter (3-dB bandwidth: 0.4 nm) to remove the amplified spontaneous emission of the EDFA before being launched into the microdisk. The back reflection from the microdisk is recorded either by a fast optical oscilloscope (3-dB bandwidth: 30 GHz) to observe its temporal waveform or by an optical spectrum analyzer (resolution: 15 pm) to observe its spectrum.

3. Observation of adiabatic self-tuning

We first launch 2-ns square pulses [Fig. 2(a)] into a resonance at 1542.94nm. A continuous-wave linear scan of its transmission spectrum [Fig. 2(e)] shows that the two modes of the doublet have an average intrinsic and loaded Q factor [17] of 1.4×10^6 and 9.2×10^5, respectively, corresponding to a loaded photon lifetime of 753 ps. At a low input power of 78 μW, the cavity behaves linearly and its reflection wave shows a clear resonance buildup and ringdown [Fig. 2(b)]. However, when the input power increases, TPA-generated free carriers dynamically tune the cavity resonance during the resonance buildup, and the reflected signal starts to oscillate significantly across its entire temporal waveform. With an input peak power of 2.5 mW [Fig. 2(c)], the waveform exhibits a clear oscillatory pattern with a period of about 550 ps. The oscillation period decreases monotonically with increased input power. For example, it reaches a value of about 160 ps at a power level of 40 mW [Fig. 2(d)]. In addition, a clear increase in the oscillation period across the length of the pulse is visible at the higher power levels [see Fig. 2(d), where the period increases to 278 ps at the pulse tail]. As discussed below, this time-dependent variation of the oscillation period stems from the adiabatic back tuning of cavity resonance introduced by the carrier-density decay within the photon lifetime.

The temporal oscillations imply the generation of new frequency components, as shown clearly in Fig. 2(f). A blue-shifted frequency component is generated, whose frequency shift directly corresponds to the observed temporal oscillation period. The frequency shift increases with increased power, with a slope efficiency in the range of $1.4-0.25$ pm/mW, depending on the input power level. This slope efficiency is significantly higher than that obtained through external tuning, which generally requires a peak power greater than 1 Watt even for pumping above the silicon bandgap [6–8, 11]. Although TPA in the telecom band is much weaker than the direct single-photon absorption above the silicon bandgap, the dramatic cavity enhancement enabled by the high Q factor helps substantially reduce the power requirement for dynamical cavity tuning. On the other hand, Fig. 2(f) shows that the magnitude of the blue-shifted component decreases with increased frequency shift. This is a result of the fact that, apart from the tuning of cavity resonance, TPA-induced free carriers also perform a dynamic self-tuning of the cavity Q-factor through free-carrier absorption (FCA) which reduces the number of blue-shifted trapped photons.

4. Theoretical modeling

The observed phenomena are well described by the following model governing the nonlinear field dynamics inside the silicon microdisk. The intracavity fields satisfy the dynamic equations as [15, 18]:

$$\frac{dE_f}{dt} = i(\omega-\omega_0)E_f - \frac{E_f}{2\tau_t} + i\beta_0 E_b + \Gamma\left(\frac{i\omega n_{\rm f}}{n_0} - \frac{c\alpha_{\rm f}}{2n_0}\right)E_f + i\gamma(|E_f|^2+2|E_b|^2)E_f + \frac{iE_i}{\sqrt{\tau_e}}, \quad (1)$$

$$\frac{dE_b}{dt} = i(\omega-\omega_0)E_b - \frac{E_b}{2\tau_t} + i\beta_0 E_f + \Gamma\left(\frac{i\omega n_{\rm f}}{n_0} - \frac{c\alpha_{\rm f}}{2n_0}\right)E_b + i\gamma(|E_b|^2+2|E_f|^2)E_b, \quad (2)$$

where E_f, E_b, and E_i are the slowly-varying field amplitudes of the forward and backward WGMs and the input wave, respectively, normalized such that $|E_j|^2$ ($j=f,b$) represents the

#98656 - $15.00 USD Received 11 Jul 2008; revised 1 Sep 2008; accepted 1 Sep 2008; published 4 Sep 2008

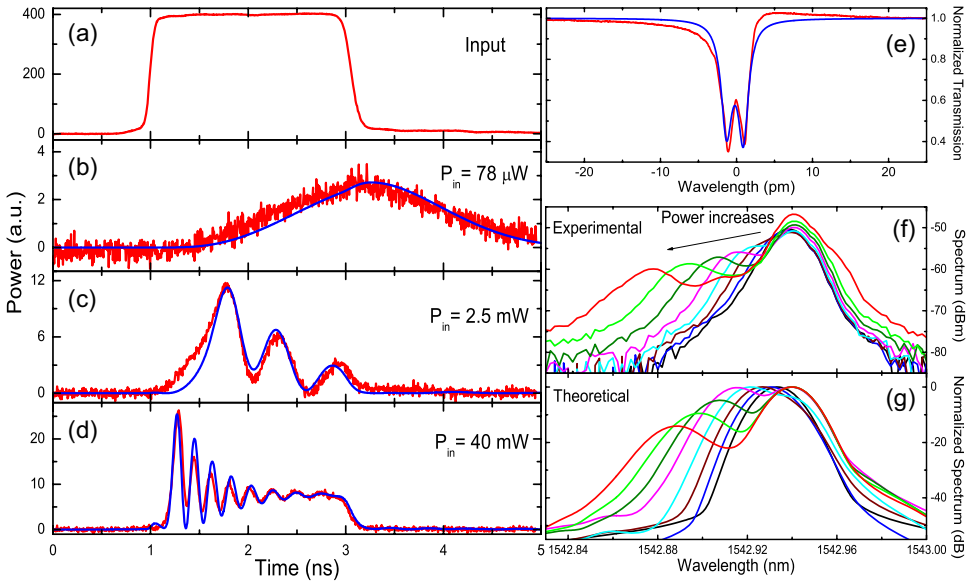

Fig. 2. (a) The input pulse waveform. (b)-(d) Recorded (red) and simulated (blue) temporal waveforms of the back reflected fiber taper signal from the cavity at the three different power levels. The input pulse has a carrier wavelength resonant with the doublet at $\lambda = 1542.94$ nm. (e) Low power (linear regime) transmission wavelength scan of the doublet resonance (red: experimental record; blue: theoretical fitting). The doublet has an average intrinsic and loaded Q factor of 1.4×10^6 and 9.2×10^5, respectively. (f) Recorded and (g) simulated optical spectra at input power levels varying from 0.63 to 80 mW. The input power is doubled in each successive curve. The finite spectral resolution of the OSA (15 pm) has been incorporated into the theoretical spectra in (g), where the spectral response of the OSA is assumed to have a Gaussian shape. In (g), each theoretical spectrum is normalized by its own maximum.

intracavity field energies but $|E_i|^2$ represents the input power. In Eqs. (1) and (2), the first term on the right side represents the detuning of the input carrier frequency ω with respect to the cavity resonance ω_0. The second term governs the photon decay inside the cavity with a lifetime τ_t of the loaded cavity. The third term describes the mode coupling between the forward and backward WGMs, with a coupling coefficient of β_0. The doublet shown in Fig. 2(e) exhibits a mode splitting of 2.29 pm, corresponding to $\beta_0 = 0.91$ GHz. The final term of Eq. (1) represents the power feeding from the input wave, where τ_e is the photon escape time associated with the external coupling. In Eqs. (1) and (2), $n_0 = 3.48$ is the material refractive index of silicon and Γ is the confinement factor of the energy inside the microdisk. $\Gamma \approx 1$ for the TE-like resonances.

The Kerr nonlinear effects are governed by the fifth term with a nonlinear parameter of $\gamma = \frac{v_g^2}{V_{\text{eff}}}(\frac{\omega n_2}{c} + \frac{i\beta_T}{2})$, where n_2 and β_T are Kerr and TPA coefficients, respectively, v_g is the group velocity, and V_{eff} is the effective mode volume [12, 15, 18]. Finite element simulations of our disk show that the WGMs have a group index of 3.7 and an effective mode volume of 13.1 μm^3. Detailed analysis shows that the Kerr nonlinear effects are negligible in the adiabatic self-tuning process, compared with the dominant carrier-induced effects. The latter are governed by the fourth term, where the carrier-induced refractive index change n_{f} and absorption α_{f} are given by [19]: $\alpha_{\text{f}}(t) = \rho_\alpha 1.45(\lambda/\lambda_r)^2 N(t)\times10^{-17}$ and $n_{\text{f}}(t) = -\rho_n(\lambda/\lambda_r)^2[8.8\times10^{-4}N + 8.5N^{0.8}]\times10^{-18}$, where $\lambda_r = 1550$ nm and the carrier density N (in units of cm^{-3}) satisfies

#98656 - $15.00 USD Received 11 Jul 2008; revised 1 Sep 2008; accepted 1 Sep 2008; published 4 Sep 2008

[12, 15]

$$\frac{dN}{dt} = \frac{v_g^2 \beta_T}{2\hbar\omega V_{\text{eff}}^2}\left(|E_f|^4 + 4|E_f|^2|E_b|^2 + |E_b|^4\right) - \frac{N}{\tau_0}, \tag{3}$$

with an effective carrier lifetime of τ_0 and a TPA coefficient of $\beta_T = 0.5$ cm/GW. In the expressions of α_{f} and n_{f}, the two factors ρ_α and ρ_n are correction factors (based upon fitting to the measured data) for the magnitude of carrier effects relative to the empirical model of Ref. [19]. They also include all possible uncertainties in the TPA coefficient, effective mode volume, group velocity, etc., which may affect the magnitude of generated carrier density. Our modeling of the experimental results indicates $\rho_\alpha = 1.5$ and $\rho_n = 0.55$.

A detailed characterization of our experimental system shows that the back reflection signal has a second source in addition to the already discussed high-Q backward WGM of the microdisk. The second component of the reflected signal stems from coupling of the input wave to low-Q background modes of the microdisk. Parasitic coupling to these modes is generally unavoidable in the microdisk geometry due to the large number of higher-order radial modes. Due to their short photon lifetimes and broad spectral features, coupling to the background disk modes results in a nearly frequency independent direct reflection signal proportional to the input wave. The presence of background modes of the disk was confirmed by tuning off-resonance from the high-Q cavity modes and measuring the reflected signal. The magnitude of the detuned reflected signal was found to be $|\eta|^2 = (0.013)^2$ of the input pulse power (with the fiber taper detached from the disk the reflected signal was negligible). Taking into account both components of the reflected signal, the total back-reflected wave is then given by $E_r = \eta E_i + iE_b/\sqrt{\tau_e}$, where $|E_r|^2$ has a unit of optical power. Comparison of the measured reflected waveform to the above model indicates that $\eta = 0.013i$, where the relative $\pi/2$ phase shift is introduced by the superposition of background disk modes with various detunings from the input wave frequency.

The experimentally recorded input pulse [Fig. 2(a)] is used as the input waveform for simulation. The simulated temporal waveforms are plotted in Fig. 2(b)-(d) in a direct comparison to the experimental records. Clearly, theory and experiments agree well at various power levels. These simulations indicate a carrier lifetime of 2.5 ns. Accordingly, The corresponding simulated spectra [Fig. 2(g)] show close agreement with the experimental ones [Fig. 2(f)]. The higher magnitude of the fundamental frequency component in the experimental spectra is due to the finite extinction ratio of the electro-optic modulator which introduces a nonzero power floor on the input wave.

The physical mechanism underlying the adiabatic self-tuning process can be well understood through Fig. 3, where we plot the simulated spectrograms of the intracavity forward WGM, backward WGM, the reflected wave, together with their temporal waveforms and the carrier dynamics at a power level of 40 mW. Comparing Fig. 3(a), (b), (c) and (e), we can see clearly that the forefront of the intracavity wave remains at its original frequency since negligible carriers are created before the intracavity power builds up to a significant level for efficient TPA. However, in the time window between 1.14 and 1.24 ns, carrier density increases rapidly during a short time period of $\sim$100 ps, which simultaneously detunes the cavity resonance and thus drags the frequency of trapped photons towards blue. The blue tuning of the cavity resonance starts to quench any further power input, leading to a saturation of the intracavity power at $\sim$1.24 ns. After this time, the carrier density reaches its quasi-steady state and the photon frequency stops further tuning. The trapped photons at this blue-tuned frequency thus decay at a slightly reduced photon lifetime due to FCA. For the forward WGM, there are two frequency components simultaneously circulating inside the cavity [Fig. 3(b)], leading to beating on its temporal waveform [Fig. 3(e), blue]. For the backward WGM, however, its energy is dominantly stored at the blue-shifted frequency [Fig. 3(c)] since it is scattered from the forward WGM whose frequency is blue-shifted by the cavity tuning. As a result, less oscillations appear

#98656 - $15.00 USD Received 11 Jul 2008; revised 1 Sep 2008; accepted 1 Sep 2008; published 4 Sep 2008

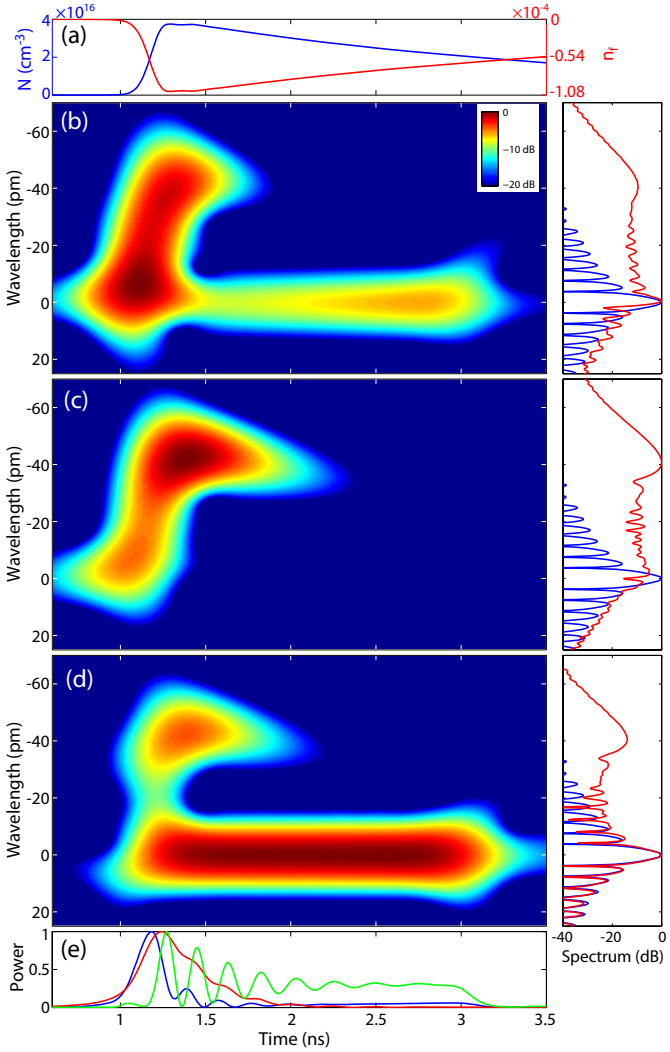

Fig. 3. Simulated spectrograms of the intracavity forward WGM (b), backward WGM (c), reflected wave (d) for the resonance of 1542.94 nm shown in Fig. 2, at an input peak power of 40 mW. The spectrograms are plotted in a log scale. The right column shows the corresponding spectra (red) compared with the input (blue). The impact of the OSA resolution is not incorporated into the spectra. (e) shows the normalized temporal waveforms for the three waves (blue: forward WGM; red: backward WGM; green: reflected wave). (a) shows the carrier density N (blue) and induced refractive-index change n_f (red). The sampling time window is 400 ps for the spectrograms.

in its temporal waveform [Fig. 3(e), red].

After quasi-steady state is reached, the carrier density decays considerably within the carrier lifetime of 2.5 ns [Fig. 3(a), blue curve]. As the cavity photon lifetime is relatively long, the significant decay of the carrier density causes a second adiabatic tuning of the trapped photons, but this time tuning back towards the input frequency [Fig. 3(b) and (c)]. Consequently, the oscillation period in the time domain increases across the temporal waveform on a time

#98656 - $15.00 USD Received 11 Jul 2008; revised 1 Sep 2008; accepted 1 Sep 2008; published 4 Sep 2008

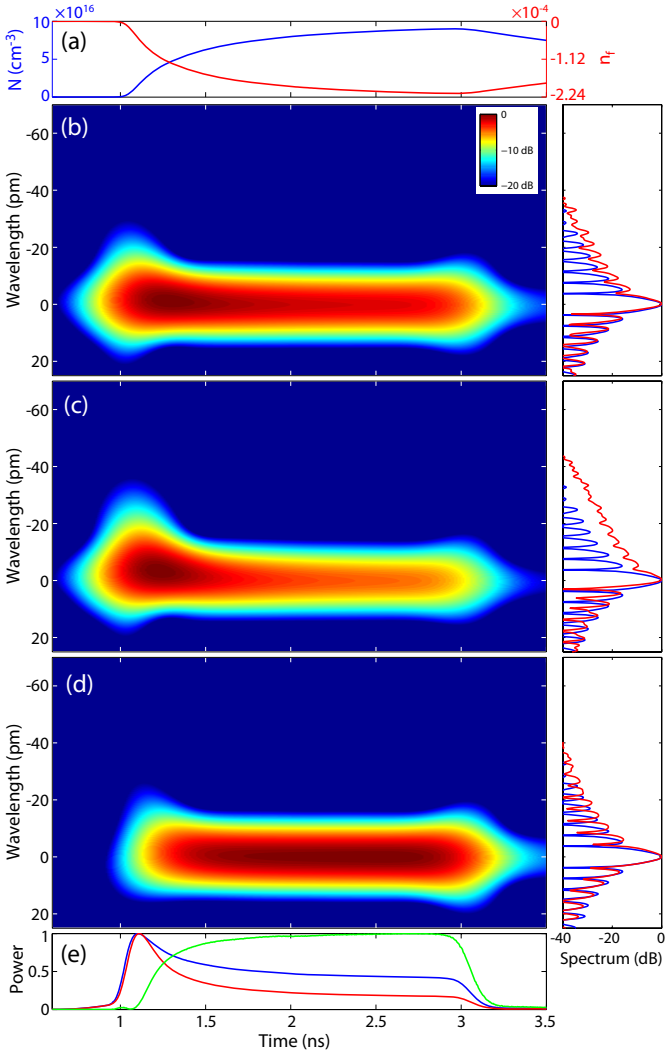

Fig. 4. Same as Fig. 3 except that the resonance is assumed to be critically coupled to the fiber taper with a loaded Q factor of 10^4 .

scale of the carrier lifetime [Fig. 3(e), blue and red]. As the reflected wave consists of two different frequency components contributed by the blue-shifted backward WGM and the directly reflected input wave [Fig. 3(d)], its temporal waveform [Fig. 3(e), green] exhibits significant oscillations with a beating magnitude even larger than that of the forward WGM. Therefore, similar to a heterodyne detection, the direct back reflection introduced by the background disk modes functions as a local oscillator to enhance the temporal beating. The beating-period variations introduced by the adiabatic back tuning is clearly imprinted across the pulse profile, exactly as what is observed in Fig. 2(d) where the oscillation period increased by about 74% towards the pulse tail. Such temporal variation of the beating period is a direct signature of cavity tuning dynamics. It can be used as an ultrafast diagnostic tool for sensitively probing the nonlinear dynamics inside high-Q microcavities. Although we used it here to probe the carrier-

#98656 - $15.00 USD Received 11 Jul 2008; revised 1 Sep 2008; accepted 1 Sep 2008; published 4 Sep 2008

density evolution, it can also be used to investigate other nonlinear cavity dynamics, *i.e.*, the opto-mechanical kinetics if the cavity tuning is introduced by opto-mechanical coupling [4]. The power requirement for adiabatic self-tuning can be further reduced by using a smaller disk, since the tuning efficiency is inversely proportional to the square of the effective mode volume [see Eq. (3)].

The adiabatic self-tuning process depends strongly on the relative magnitude of the cavity tuning time and the photon lifetime. It disappears when the latter becomes smaller than the former, where the trapped photons do not have enough time to experience the cavity tuning before dying out. Figure 4 shows a simulation result for a critically-coupled resonance with a loaded Q of 10^4, corresponding to a photon lifetime of 8 ps. Although the carrier density continuously increases to a level even higher than that for the high-Q mode shown in Fig. 3, it occurs in a time scale much longer than the photon lifetime. Consequently, the optical fields do not show a frequency shift and the oscillatory pattern is absent in their temporal waveforms, which exhibit a long pulse tail. Therefore, in practice, the adiabatic self-tuning process can be observed experimentally only in resonances with a Q factor above a certain level.

5. Applications to pulse compression and tunable delay

Figures 2 and 3 show that the quenching of power feeding introduced by the adiabatic self-tuning process leaves a dominant peak in the pulse front, with an oscillatory tail whose temporal duration depends on the cavity photon lifetime. This mechanism readily provides an efficient way for pulse compression, since the oscillatory tail can be easily suppressed by changing the cavity Q factor to reduce the photon lifetime. Figure 5 shows such an example, where we launched the same 2-ns pulses into a resonance at 1551.27nm which has a loaded and intrinsic Q factor of 1.46×10^5 and 3.28×10^5 [inset of Fig. 5(a)], respectively. At a low power of 0.18 mW when the carrier effects are negligible [Fig. 5(a), blue curve], the reflected wave exhibits a fast resonance buildup and ringdown because of the short photon lifetime of 120 ps. When the input power increases, the adiabatic self-tuning process starts to significantly compress the temporal width of the pulse. In contrast to the previous high-Q mode, the short photon lifetime suppresses considerably the oscillation in the pulse tail, leaving only a nearly symmetric squeezed pulse at the leading edge. Its full width at half maximum reaches a value of 156 ps at the power level of 22.4 mW [Fig. 5(a), red curve], which is about one order of magnitude smaller than the carrier lifetime. The compressed pulse width decreases further with higher input power. In principle, the generated pulse duration is ultimately limited only by the cavity round-trip time since the quenching speed of the external power feeding is determined by the magnitude of the carrier-induced extra phase shift per round trip.

Figure 3 shows that the onset of adiabatic self-tuning is determined by the time when the carrier density starts a rapid growth. As the carrier-density growth depends on the power feeding process, which itself is affected by the frequency detuning from the cavity resonance, we can use the detuning to control the temporal delay of the squeezed pulse. This is shown in Fig. 5(b). When the input wavelength is detuned by about 16 pm on the blue side of the resonance, the intracavity power only grows slowly in the beginning along with the adiabtic tuning of the cavity resonance. However, as the plasma-dispersion effect moves the resonance towards the input wavelength, the power feeding accelerates with time until a point where fast adiabatic self-tuning occurs and generates a squeezed pulse. Consequently, the generated pulse is delayed by 115 ps [Fig. 5(b), blue curve] compared with the on-resonance case [Fig. 5(b), red curve]. The magnitude of time delay can be controlled by the input power as well as the frequency detuning. For example, it increases to 309 ps when the input power reduces to 5.6 mW. Therefore, adiabatic self-tuning provides a "slow-light" like effect for tunable time delay. In practice, a substantial increase of time delay can be realized by using a cascade configuration with mul-

#98656 - $15.00 USD Received 11 Jul 2008; revised 1 Sep 2008; accepted 1 Sep 2008; published 4 Sep 2008

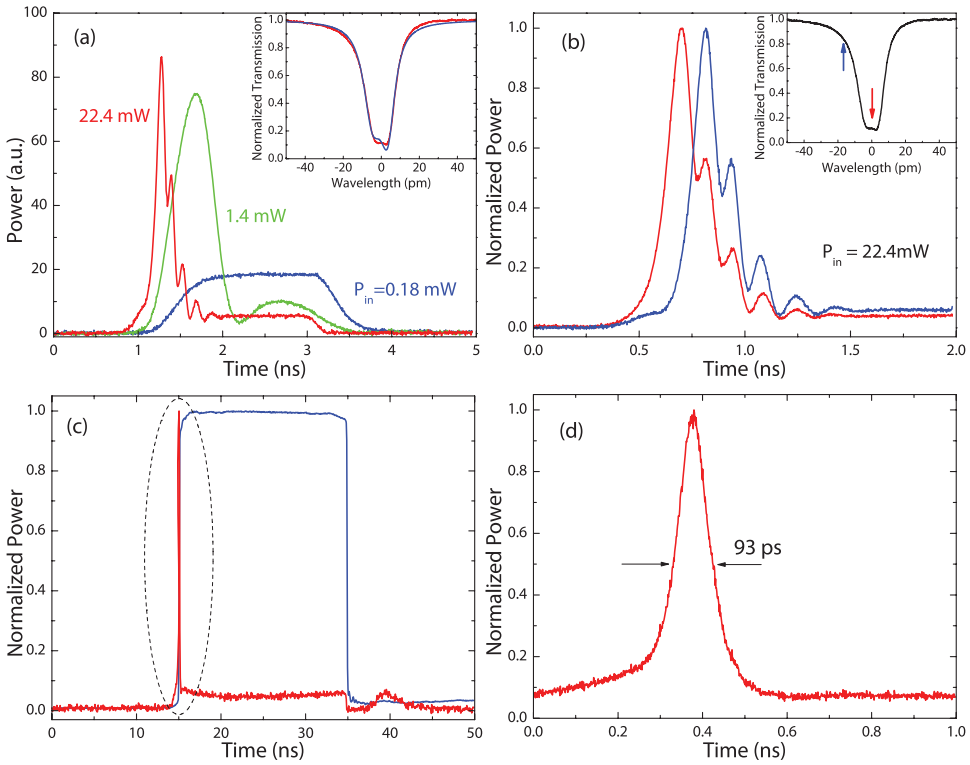

Fig. 5. (a) Recorded reflected signal temporal waveforms for excitation of the resonance at $\lambda = 1551.27$ nm under three different peak power levels. The inset shows the low-power (linear regime) transmission wavelength scan of the high-Q resonant mode (red: experimental record; blue: theoretical fitting). The doublet has an average intrinsic and loaded Q factor of 3.28×10^5 and 1.46×10^5, respectively. (b) Reflected signal temporal waveforms recorded with different frequency detuning, as indicated by the red (on-resonance) and blue (16 pm blue-detuned) arrows in the inset. (c) Reflected signal temporal waveform for an input pulse of 20 ns with a peak power of 20.5 mW launched on-resonance with a cavity mode of loaded $Q = 9.7 \times 10^4$. The blue and red curves are for the input and reflection signals, respectively. A small hump at $t = 40$ ns is due to the non-zero floor of the tail of the input pulse (a result of the limited optical modulator extinction). A zoomed-in view of the measured compressed pulse waveform [indicated by the dashed circle in (c)] is shown in (d).

tiple cavities. Moreover, as the initial frequency detuning primarily delays the fast adiabatic self-tuning process but changes little its detailed dynamic behavior, the generated pulses are of similar pulse profile independent of detuning, as shown in Fig. 5(b). The "slow-light" effect introduced by adiabatic self-tuning suffers little from the dispersion-induced pulse distortion common in other slow-light optical systems [20, 21].

Note that the pulse squeezing and shaping is determined only by the fast adiabatic self-tuning process occurring during the resonance buildup. As a result, an identically squeezed pulse would be generated independent of the input pulse length (limited, ultimately, by the free-carrier lifetime and relaxation of the cavity back to its original resonance frequency). Figure 5(c) and (d) show an example of the squeezed pulse from a 20-ns input pulse launched into a resonance with a loaded Q of 9.7×10^4. The adiabatic self-tuning process dramatically

#98656 - $15.00 USD Received 11 Jul 2008; revised 1 Sep 2008; accepted 1 Sep 2008; published 4 Sep 2008

compresses the pulse waveform, leaving only a sharp spike at the leading edge. The full width at half maximum of the compressed pulse is only 93 ps, corresponding to a temporal squeezing factor of more than 200. From an application point of view, the adiabatic self-tuning process provides an efficient way for flexible pulse compression, with a compressed pulse width continuously tunable by input peak power, and an efficiency more than two orders of magnitude higher than the scheme based on FCA inside a silicon waveguide [22].

6. Conclusion

We have demonstrated a novel approach for dynamically tuning a silicon microdisk resonator, and used it to realize various optical functionalities like pulse compression, shaping, and tunable time delay. As the compressed pulse shape is primarily determined by the cavity tuning dynamics, it is fairly insensitive to temporal distortion and fluctuations on the input pulse and thus may provide an efficient way for signal regeneration. Additional refinement of the compressed pulse shape can be realized by optimization of the cavity *Q*-factor. Although we use the back reflection from the microdisk to demonstrate the phenomena, in practice, a second fiber taper or bus waveguide can be used as a drop port for more effective extraction of the compressed pulse. On the other hand, the device can be placed in a cascade configuration for multi-channel operation. In particular, in contrast to other carrier-based signal modulation schemes [23, 24] whose modulation speeds are primarily limited by the carrier lifetime, the adiabatic self-tuning process does not suffer from such a carrier-lifetime bottleneck. While the repetition rate of the processed signal may be affected by the carrier lifetime, it can be significantly improved by various carrier-lifetime engineering techniques. Therefore, our demonstrated scheme may find useful applications in optical packet switching, label swapping, channel routing, etc., in future high-speed integrated photonic interconnects.

Acknowledgment

The authors would like to thank Jidong Zhang, Matt Eichenfield, Raviv Perahia, and Paul Barclay for helpful discussions. This work is supported by Defense Advanced Research Projects Agency (DARPA) under the programs of Parametric Optical Processes and Systems (POPS) and Electronic and Photonic Integrated Circuits (EPIC).

#98656 - $15.00 USD Received 11 Jul 2008; revised 1 Sep 2008; accepted 1 Sep 2008; published 4 Sep 2008